Journal of Power Sources 185 (2008) 143–152

Contents lists available at ScienceDirect

Journal of Power Sources

journal homepage: www.elsevier.com/locate/jpowsour

Optimum geometrical design for improved fuel utilization in membraneless micro fuel cell

Dewan Hasan Ahmed, Hong Beom Park, Hyung Jin Sung*

Department of Mechanical Engineering, KAIST, 373-1, Guseong-dong, Yuseong-gu, Daejeon 305-701, Republic of Korea

ARTICLE INFO

Article history:
Received 29 March 2008
Received in revised form 22 May 2008
Accepted 5 June 2008
Available online 25 June 2008

Keywords:
Membraneless micro fuel cell
Portable application
Trident-shaped design
Mixing width
Depletion width
Fuel utilization

ABSTRACT

In membraneless micro fuel cells, the mixing and depletion widths are major factors that determine the cell performance. Cells in which these widths are too large exhibit severely reduced fuel utilization and, hence, less electrochemical reaction especially in the downstream region of the channel. For cells with conventional rectangular geometry, increasing the aspect ratio reduces the mixing width but reduces the effective electrode area. This work proposes a trident-shaped geometrical design for membraneless micro fuel cells in which the anode fluid, cathode fluid and proton-conducting fluid are introduced through three distinct inlets. The anode and cathode fluids are interconnected by the proton-conducting fluid channel. In addition, the anode fluid and proton-conducting fluid are connected by a small narrow passage, and the cathode fluid and proton-conducting fluid channel are also connected by a small narrow passage. Numerical simulations, including the effects of electrochemical reaction and fluid flow, are carried out to investigate reactant distributions in the downstream region of the channel and to study fuel utilization. A fuel utilization of around 51% is achieved when the two opposite walls are used as reaction surfaces and the inlet velocity is set at 0.01 m s^{-1}. By varying the cell length and expanding the reaction surface areas by including additional surfaces within the cell, simulations show that the fuel utilization can be improved to around 86%, which is much higher than has been achieved in previous studies. The present numerical results are validated by comparison with available literature data.

1. Introduction

The membraneless micro fuel cell is one of the new technologies in the fuel cell arena. This type of fuel cell is considered as a prospective power source for portable devices in which liquid fuel and oxidant are used as energy sources. The demand for portable electronic devices is increasing, and is expected to accelerate. Major concerns for portable devices (e.g., cell phones, laptops, global positioning systems, cameras, and appliances for medical diagnostic and military applications) are the electrical energy source and the device size and weight. At present, the proton-exchange membrane fuel cell (PEMFC) and the direct methanol fuel cell (DMFC) are considered as candidates for portable micro fuel cells. However, PEMFCs and DMFCs both rely on a membrane and there are several problems associated with their operation that include water management and carbon monoxide production that could potentially poison the catalyst. Moreover, attempts to miniaturize fuel cells give rise to other challenges, e.g., water removal and crossover of reactants [1]. In addition, geometrical aspects such as the channel shoulder width are also a major concern with respect to the concentration overpotential [2,3]. In general, the membrane is the key component of PEMFCs and DMFs and accounts for around 15% of the total cost of the cell. The membrane electrode assembly (MEA), which comprises the electrodes and membrane, accounts for around 50% of the total cost [4]. Thus, developing a membraneless micro fuel cell would be greatly beneficial for portable device technologies as such a cell would eliminate or reduce the above problems.

In a membraneless micro fuel cell, the liquid reactants (fuel and oxidant) flow side by side in a single channel without a membrane or any separation of the materials. Such flow is usually laminar through a small channel. Two electrodes are positioned in the opposing two side walls of the single channel. Many experimental studies have been carried out to improve the specific power of membraneless micro fuel cells. Various fuel and oxidant compositions have been tested, for example, H_2 dissolved in H_2SO_4 or H_2 dissolved in KOH as the fuel along with O_2 dissolved in H_2SO_4 as the oxidant [5]; and formic acid (HCOOH) in H_2SO_4 as the fuel and O_2 dissolved in $KMnO_4$ and H_2SO_4 as the oxidant [6]. Other studies have considered vanadium redox species [7], H_2O_2 [8], and methanol (CH_3OH) [9] as the fuel to obtain higher power density. Dissolved oxygen has been the oxidant of choice in previous

* Corresponding author. Tel.: +82 42 869 3027; fax: +82 42 869 5027.
E-mail address: hjsung@kaist.ac.kr (H.J. Sung).

0378-7753/$ – see front matter © 2008 Elsevier B.V. All rights reserved.
doi:10.1016/j.jpowsour.2008.06.045

Nomenclature

A	pre-exponential constant (s^{-1})
C	concentration ($mol\,m^{-3}$)
d	height of the anode or cathode fluid channel (mm)
D	diffusion coefficient ($m^2\,s^{-1}$)
D_h	hydraulic diameter of the channel cross-section (mm)
E_a	activation energy ($kJ\,mol^{-1}$)
F	Faraday constant, 96,487 ($C\,mol^{-1}$)
h	height of the proton-conducting fluid channel (mm)
H	height of the geometry (mm)
H_0	maximum height of the geometry (mm)
j_0	exchange-current density ($A\,m^{-2}$)
L	length of the channel (mm)
L_0	maximum length of the channel (mm)
n	temperature exponent
P	net rate of production of species by chemical reactions
Pe	Peclet number (UH/D)
R	gas constant ($8.314\,J\,(mol\,K)^{-1}$)
T	temperature (K)
U	velocity ($m\,s^{-1}$)
W	width of the geometry (mm)
W_0	maximum width of the geometry (mm)
x	distance (mm)
Y	species mass fraction

Greek letters

α	charge-transfer coefficient
η	overpotential (V)
μ	viscosity ($N\,s\,m^{-2}$)
σ	electrical conductivity ($S\,m^{-1}$)

studies on membraneless micro fuel cells. The use of dissolved oxygen, which has a low diffusivity in aqueous solution, means that mass transfer of oxidant to the cathode is a factor limiting cell performance. In practice, the low diffusivity of oxygen causes severe problems associated with the depletion of reactants, especially oxidant, in the downstream region of the channel. Jayashree et al. [1] suggested an air-breathing laminar, flow-based, micro-fluidic fuel cell, in which air is directly used as the oxidant. Despite these developments, all membraneless micro fuel cells developed to date have maximum power densities of only a few $mW\,cm^{-2}$.

Besides choosing appropriate fuel and oxidant compositions, mixing and depletion widths are major concerns in terms of fuel cell operation. The mixing width of the two streams depends mainly on the upstream flow conditions and the geometrical structure of the channel. The operation of a micro fuel cell begins to fail when the anode and cathode fluid streams become mixed to the point where oxidation and reduction are no longer restricted to the appropriate electrodes [10]. The mixing width can be reduced by increasing the Peclet number Pe ($Pe = UH/D$), where U is the average velocity, H is the height of the channel, and D is the diffusivity of the species [11]. Increasing U means increasing the flow rate, which in turn increases the consumption of fuel and oxidant. One possible way to reduce the mixing width is to optimize the geometrical design such that there is less mixing. The mixing width also depends on the height of the channel ($\Delta z = (DHx/U)$), where x is the distance that the fluid flows downstream. As a result, a cell with a higher aspect ratio (width:height) will have a smaller mixing width. The depletion of reactants (fuel and oxidant) near the electrodes, quantified as the depletion width, is another key difficulty in the downstream of the channel, and leads to a lowering of the cell performance. The depletion width is also affected by the mixing of the two streams in the main channel. In addition, formation of a depletion boundary layer means that excess reactants never reach the electrode surface, leading to a low conversion rate. It is emphasized that the concentration boundary layer thickness should be as small as possible to create a steeper concentration gradient at the electrode surfaces. A steep concentration gradient generates a large driving flux of reactants through the depletion zone and thereby increases the conversion rate of the chemical reaction and thus the cell performance [6]. Moreover, the depletion of reactants also depends on the fluid compositions in the anode and cathode channels; this is especially true for systems with oxygen dissolved in aqueous solution, as oxygen is much less soluble in aqueous media to yield a concentration less than that in air. To maximize fuel utilization, the geometrical shape and structure of a membraneless micro fuel cell must therefore be designed to reduce the mixing and depletion widths of the two streams and to allow the two streams to flow in thin bands adjacent to their respective electrodes with a steeper concentration gradient.

The objective of the present study is to confine the reactants to their respective electrodes and hence to reduce the depletion width at the downstream of the main channel. To achieve this, a new design for a membraneless micro fuel cell is proposed so that the reactants are kept away from the opposite electrodes. Numerical simulations are performed using a three-dimensional model with a trident-shaped micro channel geometry. These simulations, which account for both fluid flow and electrochemical reactions at the electrodes, generate information on the flow behaviour and distributions of reactants and byproducts in the main channel. The diffusive mixing of the reactants is investigated both normal and parallel to the reaction surfaces. Moreover, the distribution of byproducts over the anode reaction surface is examined. Further, the effects of varying the inlet velocities and channel length in the proposed geometrical design are evaluated, together with the fuel utilization. The simulation results are validated by comparison with available literature data.

2. Geometrical design of membraneless micro fuel cell

In a membraneless micro fuel cell, the mixing and depletion widths gradually increase as the fluids move downstream. In general, the mixing width is smallest in the middle of the channel cross-section and maximum near the wall. This causes the mixing width to have an hour-glass shape in the channel cross-section. To resolve the performance problems discussed above, it is important to keep the reactant flows close to the electrode surfaces and to reduce the concentration boundary layer thickness of the system. To reduce or control the mixing and depletion widths along the channel length, many geometrical designs have been tested by trial and error. In one system, for example, some small blocks (spikes) were inserted in pairs to confine the mixing to the centre line of the channel, while in another system various diamond-shaped blocks were introduced in pairs along the channel length. As the mixing width did not vary significantly along the channel length, a converged–diverged situation repeatedly along the channel length was also considered by including blocks in pairs at regular intervals. On the basis of those tests, it was found that the trident-shaped geometry shown in Fig. 1 was the best, and that this geometry controlled the mixing and the depletion widths to a much greater degree than conventional geometries with rectangular cross-sections.

A top view of the trident-shaped geometry, which consists of three inlets and one outlet, is presented in Fig. 1(a). A cross-sectional view of the main channel, where the reactions occur on

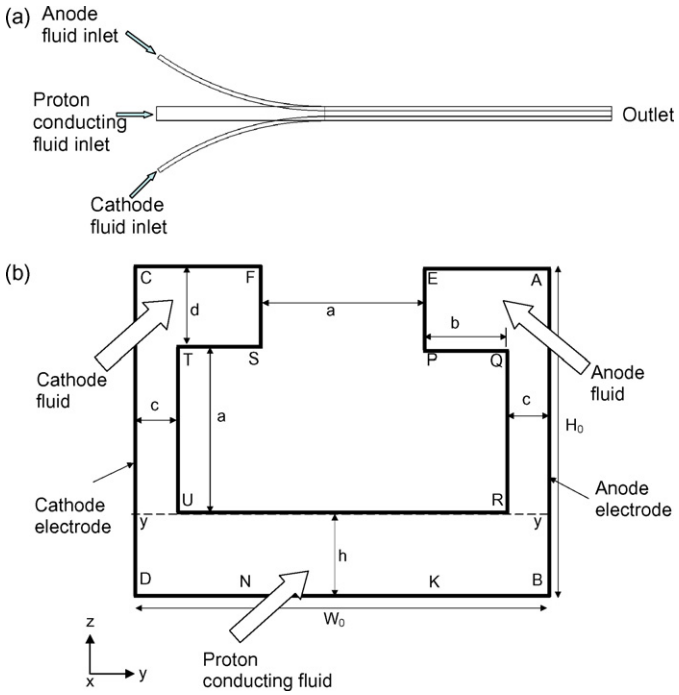

Fig. 1. Conceptual design for membraneless micro fuel cell: (a) top view and (b) cross-sectional view.

the side walls (AB and CD), is given in Fig. 1(b). The top two inlets (left and right) are for cathode and anode fluids and the bottom inlet is for proton-conducting fluid. There are two small passages: one connecting the anode fluid and proton-conducting fluid, and the other connecting the cathode fluid and proton-conducting fluid. A solid block is located inside the main channel, which restricts the fuel and oxidant from coming into direct contact. The side walls (see Fig. 1(b)) can be used as electrodes for a membraneless micro fuel cell. The present model considers only the case in which the surface reactions occur on these two side walls. The electrode area (reaction surface area) could, however, be increased by additionally using the top and bottom walls of the main channel as electrodes.

Table 2
Physical parameters and boundary conditions

Parameter	Value
Velocity at fuel inlet	0.01 m s^{-1}
Velocity at oxidant inlet	0.01 m s^{-1}
Velocity at proton-conducting fluid inlet	0.01 m s^{-1}
Diffusivity	5×10^{-10} m^2 s^{-1}
Length of main channel	10 mm
Width of main channel	0.5 mm
Activation energy for formic acid oxidation	48.57 kJ mol^{-1}
Pre-exponential constant for formic acid oxidation	15000
Activation energy for oxygen reduction	11.03 kJ mol^{-1}
Pre-exponential constant for oxygen reduction	9320
Anode exchange-current density	9×10^8 A m−2
Cathode exchange-current density	250 A m−2
Charge-transfer coefficient for oxidation	0.497
Charge-transfer coefficient for reduction	0.5

The system dimensions used in the different cells are listed in Table 1. Note that for all cases, the width (W) of the channel is fixed at a constant value of 0.5 mm, but the height and the inlet area are varied to obtain an effective distribution of reactants with respect to the electrode surfaces (or reaction surfaces). The width of the solid slab (e.g., 'a' in Fig. 1(b)) was made sufficiently large to ensure mechanical stability of the cell. The systems are divided into four sets, with each set consisting of five cases (Table 1). The cases in Table 1 are denoted using the notation 'Case *abcdh*' according to the dimensions in millimeters of '*a*', '*b*', '*c*', '*d*' and '*h*' in Fig. 1(b). For example, Case 2-13-02-15-05 corresponds to '*a*' = 0.2 mm, '*b*' = 0.13 mm, '*c*' = 0.02 mm, '*d*' = 0.15 mm and '*h*' = 0.05 mm. In the present geometrical design, the reaction surface (electrode) can be placed in two vertical side walls (AB and CD). There are, however, many possibilities to increase the reaction surface area by using surfaces such as AE, CF, EP, PQ, FS, ST, BK, and DN (see Fig. 1(b)) as reaction surfaces.

3. Numerical simulation

In membraneless micro fuel cells, the fuel and oxidant flow side-by-side in a channel, with mixing of the reactants able to occur only by diffusion. A three-dimensional model for computational analysis is developed and is based on the following assumptions: laminar flow, steady-state and isothermal flow. The electrochemical reac-

Table 1
Different case studies with related channel dimensions for a membraneless micro fuel cell

Set	Case	W	a	c	d	b	h	b/a	d/a	d/h	H	W/H
Set 1	2-1-05-1-1	0.5	0.2	0.05	0.1	0.1	0.1	0.5	0.5	1	0.4	1.25
	2-1-05-1-05	0.5	0.2	0.05	0.1	0.1	0.05	0.5	0.5	2	0.35	1.43
	2-1-05-05-1	0.5	0.2	0.05	0.05	0.1	0.1	0.5	0.25	0.5	0.35	1.43
	2-1-05-15-05	0.5	0.2	0.05	0.15	0.1	0.05	0.5	0.75	3	0.4	1.25
	2-1-05-05-15	0.5	0.2	0.05	0.05	0.1	0.15	0.5	0.25	0.33	0.4	1.25
Set 2	2-13-02-1-1	0.5	0.2	0.02	0.1	0.13	0.1	0.65	0.5	1	0.4	1.25
	2-13-02-1-05	0.5	0.2	0.02	0.1	0.13	0.05	0.65	0.5	2	0.35	1.43
	2-13-02-05-1	0.5	0.2	0.02	0.05	0.13	0.1	0.65	0.25	0.5	0.35	1.43
	2-13-02-15-05	0.5	0.2	0.02	0.15	0.13	0.05	0.65	0.75	3	0.4	1.25
	2-13-02-05-15	0.5	0.2	0.02	0.05	0.13	0.15	0.65	0.25	0.33	0.4	1.25
Set 3	1-15-05-1-1	0.5	0.1	0.05	0.1	0.15	0.1	1.5	1	1	0.3	1.67
	1-15-05-1-05	0.5	0.1	0.05	0.1	0.15	0.05	1.5	1	2	0.25	2
	1-15-05-05-1	0.5	0.1	0.05	0.05	0.15	0.1	1.5	0.5	0.5	0.25	2
	1-15-05-15-05	0.5	0.1	0.05	0.15	0.15	0.05	1.5	1.5	3	0.3	1.67
	1-15-05-05-15	0.5	0.1	0.05	0.05	0.15	0.15	1.5	0.5	0.33	0.3	1.67
Set 4	1-18-02-1-1	0.5	0.1	0.02	0.1	0.18	0.1	1.8	1	1	0.3	1.67
	1-18-02-1-05	0.5	0.1	0.02	0.1	0.18	0.05	1.8	1	2	0.25	2
	1-18-02-05-1	0.5	0.1	0.02	0.05	0.18	0.1	1.8	0.5	0.5	0.25	2
	1-18-02-15-05	0.5	0.1	0.02	0.15	0.18	0.05	1.8	1.5	3	0.3	1.67
	1-18-02-05-15	0.5	0.1	0.02	0.05	0.18	0.15	1.8	0.5	0.33	0.3	1.67

tions of the reactants occur only at the electrodes. The following governing equations, which include conservation of mass, momentum transport and species transport equations, are solved for the numerical simulations:

$$\nabla \cdot (\rho \vec{u}) = 0. \quad (1)$$

$$\nabla \cdot (\rho \vec{u}\vec{u}) = -\nabla P + \nabla \cdot (\mu \nabla \vec{u}). \quad (2)$$

$$\nabla \cdot (\rho Y_i \vec{u}) = \nabla \cdot (J_i) + P_i. \quad (3)$$

where Y_i is the species mass fraction of species i, and P_i is the net rate of production of species i by chemical reaction. The species mass flux is given by:

$$J_i = -\rho D_i \nabla Y_i, \quad (4)$$

where D is the diffusion coefficient.

For this study, formic acid and dissolved oxygen in sulfuric acid solution are chosen as the fuel and oxidant, respectively. The oxidation of the formic acid at its reaction surface (the anode) is:

$$2HCOOH \rightarrow 2CO_2 + 4H^+ + 4e^- \quad (5)$$

The reduction of oxygen at the cathode side reaction surface is

$$(6) O_2 + 4H^+ + 4e^- \rightarrow 2H_2O$$

Only the forward reactions are considered for this model, and the rate coefficients are assumed to have an Arrhenius form:

$$k = A\, e^{-E_a/RT} \quad (7)$$

where A is the pre-exponential constant; E_a is the activation energy; R is the gas constant. The pre-exponential constant and activation energy for the formic acid oxidation and the oxygen reduction reactions depend on both temperature and operating potential [12–17]. For formic acid oxidation, the pre-exponential constant and activation energy are taken as 15,000 1 s^{-1} and 48.57 kJ mol^{-1}, respectively [12]. For oxygen reduction, the pre-exponential constant and activation energy are taken as 9320 1 s^{-1} and 11.03 kJ mol^{-1}, respectively [16]. Note that we have tried to choose the values of reaction parameters for slow reactions as we have only considered the fluid flow and chemical reaction in order to investigate the mixing of the fluids and fuel utilization.

Details of the boundary conditions for the model are given in Table 2. In the present study, 0.5 M HCOOH in 0.1 M H_2SO_4 is used as the fuel [6], 1.25 mmol O_2 dissolved in 0.1 M H_2SO_4 is used as the oxidant [6,18] and 0.1 M H_2SO_4 senes as the proton-conducting fluid. The fuel, oxidant and proton-conducting fluid are introduced into the main channel via the three inlets of the trident-shape geometry.

The rate law for HCOOH oxidation is given by:

$$r = k[\mathrm{HCOOH}]^x \exp\left(\frac{\alpha_a n F \eta}{RT}\right) \quad (8)$$

where [HCOOH] is the concentration of HCOOH; x is the reaction order; α_a is the anode charge-transfer coefficient; n is the number of electrons released for particular reaction step; F is the Faraday constant; η is the overpotential. Similarly, the rate law for the oxygen reduction reaction is expressed as:

$$r = k[O_2]^x \exp\left(-\frac{\alpha_c n F \eta}{RT}\right) \quad (9)$$

where $[O_2]$ is the concentration of O_2, and α_c is the cathode charge-transfer coefficient. An additional electric potential equation is solved to obtain the electric field in the cell and is defined as

$$\sigma_i \nabla \Phi_i = S_i \quad (10)$$

where σ_i is the electric conductivity, and Φ is the electric voltage of the cell. The source term S_i is given in the form of Butler–Volmer equation, i.e.,

$$S_i = a j_0 \left(\frac{C_i}{C_{i,\mathrm{ref}}}\right)^{\beta_i} \left[\exp\left(\frac{\alpha_a n F \eta}{RT}\right) - \exp\left(-\frac{\alpha_c n F \eta}{RT}\right)\right] \quad (11)$$

where a is the specific area of the electrode per unit volume; j_0 is the exchange-current density; C_i is the concentration of species i. Note that the source terms are only active on the porous electrodes. The electric conductivity of the porous media is kept constant at, $\sigma_i = 300$ S m^{-1}. The conductivity of the electrolytes which is mainly

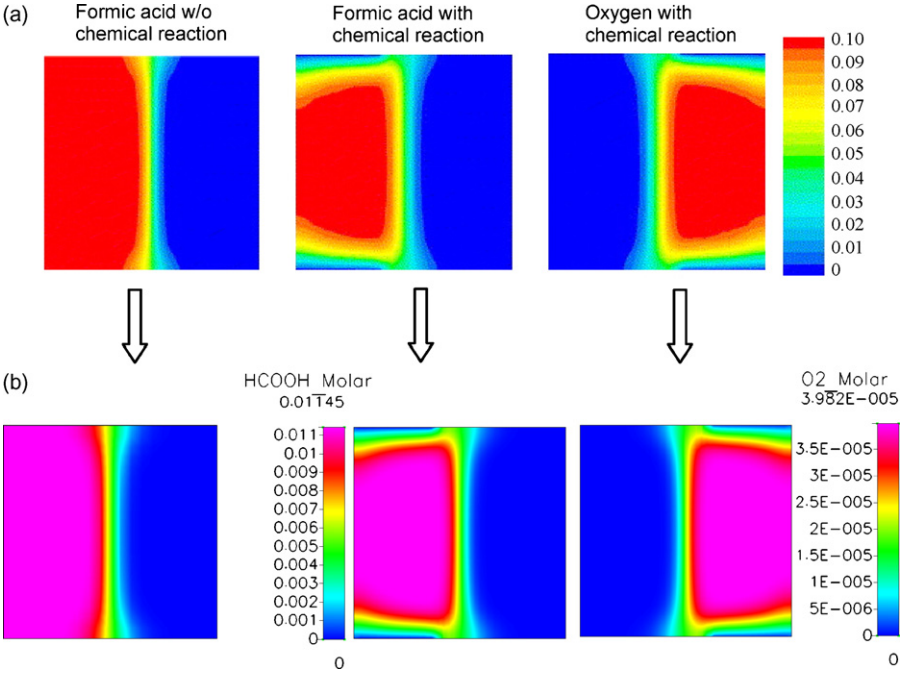

Fig. 2. Reactants distribution without and with electrochemical reaction for conventional geometry of membraneless micro fuel cell with square cross-section. (a) Bazylak et al. [11] and (b) present study.

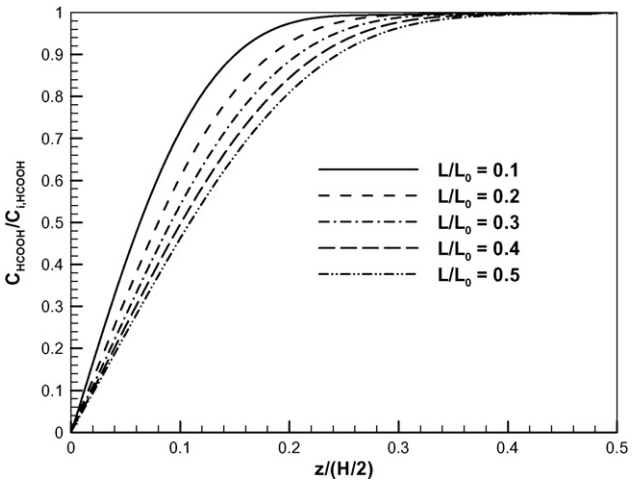

Fig. 3. Formic acid distribution normal to reaction surface for square channel geometry.

sulfuric acid, varies with the concentration of the solution itself. The conductivity of the electrolyte is defined from the sixth-order polynomial for sulfuric acid mol percentage in a solution [19].

The above governing equations are solved using the finite volume method, with appropriate boundary conditions, and employs the AMG (Algebraic Multi Grid) solver to solve the pressure correction. For all the case studies, the minimum number of cells used is 400,000, which is sufficient to fulfill the convergence criterion.

4. Results and discussion

Before proceeding further, it is important to ascertain the reliability and accuracy of the simulations. To do this, simulations were performed using a square cross-sectional geometry of the main channel [10]. Fig. 2 shows the distributions of formic acid and oxygen 6 mm downstream of the first mixing point. Fig. 2(a) gives the mass fractions of formic acid that have not undergone chemical reaction and of formic acid and oxygen that have undergone chemical reaction 6 mm downstream of the first mixing point reported by Bazylak et al. [10]. In a similar manner, Fig. 2(b) shows the corresponding distributions obtained in the present study. Comparison of the two sets of data reveals some discrepancies between the distributions of the reactants, that can be attributed to the use of different values of the various physical parameters. In general, however, the agreement is acceptable. The fuel utilization obtained in this investigation for square geometry is around 4%, which is close to the value of 3% reported by Bazylak et al. [10]. The distribution of the molar concentration of formic acid normal to the reaction surface (anode) is presented in Fig. 3. The molar concentration of formic acid is close to zero at the anode wall and suggests that the chemical reaction takes place at the electrode by developing a concentration boundary layer. This trend is similar to that reported by Bazylak et al. [10] for fuel distribution normal to the wall.

Fig. 4 gives the distributions of the molar concentration of formic acid in the main channel 8 mm downstream from the first mixing point when the model is solved without (Fig. 4a) and with (Fig. 4b) chemical reactions for Case 2-1-05-1-1. It should be noted that the two side walls were considered as electrodes when the model was solved with chemical reactions. It is clear that formic acid is reacting over most of the reaction surface. However, the distribution of formic acid shows that it does not have sufficient time to mix with the proton-conducting fluid as the mixing also depends on the diffusion coefficients and fluid velocities. Although the proton-conducting fluid is only considered to carry protons from the anode to the cathode, this diffusion can contribute significantly to the uniform distribution of the formic acid and oxygen over their respective reaction surfaces.

With the geometrical design considered in the present work, it is important that the reactants to be uniformly distributed over the respective reaction surfaces. For this to be the case, there should be active diffusion parallel to the reaction surfaces (electrodes) but less diffusion normal to the reaction surfaces. Fig. 5 shows the distributions of the molar concentrations of formic acid and carbon dioxide (byproduct) parallel to the reaction surface for the five cases of Set 1. Note that the molar concentrations of formic acid and carbon dioxide are normalized by the inlet molar concentration of formic acid. Case 2-1-05-1-1 and Case 2-1-05-05-1 have the most uniform distributions of formic acid over the reaction surface (Fig. 5(a)). By contrast, Case 2-1-05-1-05 and Case 2-1-05-15-05 exhibit the worst formic acid distributions as little carbon dioxide has been produced, see Fig. 5(b). The data is given in Fig. 5(b) imply however, that for $d/h \leq 1$ (where d/h is the ratio of the anode or cathode channel height to the proton-conducting fluid channel height) much better mixing of the anode fluid and proton-conducting fluid is possible through the small passage. Note that there is a pressure gradient in the small passage at the most upstream position of the main channel and fluid moves from the anode channel to the proton-conducting fluid channel for $d/h < 1$, and vice versa. This fluid movement among the channels influences the reactant distributions.

Fig. 6 shows the pressure distribution along the height at 0.1 mm downstream of the first mixing point at the middle of the anode small passage for the different cases of Set 1. For the systems with

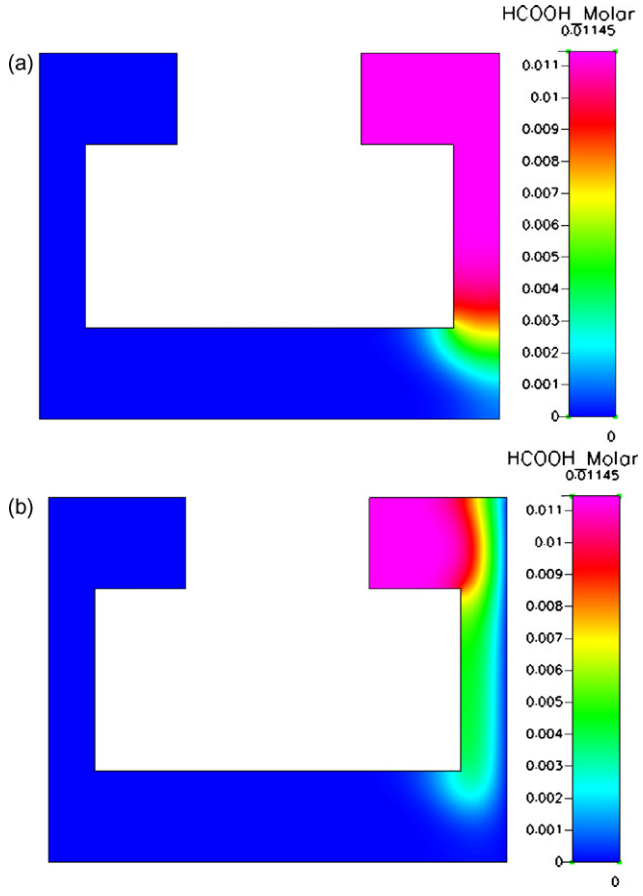

Fig. 4. Formic acid molar concentration over anode reaction surface for Case 2-1-05-1-1: (a) without reaction; (b) with reaction.

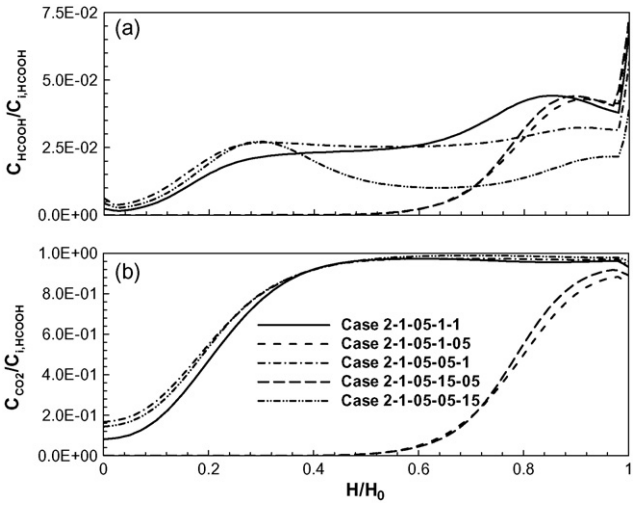

Fig. 5. Reactant molar concentration distributions parallel to reaction surfaces for different cases of Set 1: (a) formic acid; (b) carbon dioxide.

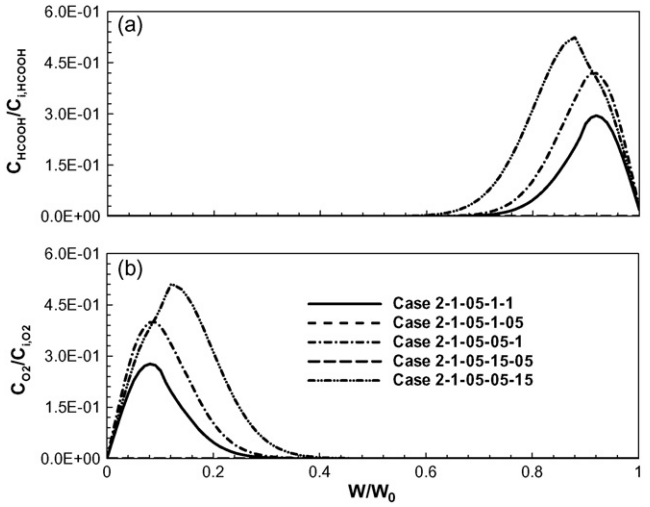

Fig. 7. Reactant molar concentration distributions normal to reaction surfaces for different cases of Set 1: (a) formic acid; (b) oxygen.

smaller heights of the anode channel (d) or the proton-conducting fluid channel (h), the pressure in a given channel is slightly higher and hence the fluid moves to the opposite channel. As a result, systems with $d/h > 1$ show non-uniform reactant distributions.

In membraneless micro fuel cells, it is important that the reactants are kept away from the opposite electrodes. This means that the system should be designed such that there is less diffusion normal to the reaction surfaces. The distributions of reactants, non-dimensionalized by their respective inlet molar concentrations, along the width of the proton-conducting fluid channel through the line y–y (see Fig. 1(b)) are presented in Fig. 7. The data clearly show that the anode and cathode fluids mainly accumulate near the small passage region and are predominantly restricted to their respective reacting surfaces for systems with $d/h \leq 1$. Note that the anode and cathode fluids each cover only around 40% of the width of the proton-conducting fluid channel and remain in their corresponding regions. For systems with $d/h > 1$, however, the formic acid and carbon dioxide do not show any remarkable mixing at the proton-conducting fluid channel, as mentioned above. With the conventional rectangular cross-sectional geometry, the anode and cathode fluids each usually occupy half of the cross-sectional area. As long as the fluid moves downstream, the anode and cathode fluids also move towards the opposite electrodes. In this situation, the anode or cathode fluid will cover more than 50% of the main channel width. With the present geometrical design with $d/h \leq 1$, however, the anode and cathode fluids are kept away from the opposite electrodes, even in the downstream region of the channel.

Fuel utilization is an important aspect of micro fuel cells in that achieving effective chemical reactions over the reaction surfaces (electrodes) leads to efficient output from the cell. Fuel utilization is defined as the ratio of the total consumption rate of the fuel in the cell to the total mass flow rate of the fuel at the inlet, i.e., fuel utilization = (fuel flow rate at inlet − fuel flow rate at outlet)/(fuel flow rate at inlet). The fuel utilizations of the present geometrical design for the five cases of Set 1 given in Fig. 8. The highest fuel utilization, 51%, was achieved for Case 2-1-05-05-1. Changing the dimensions such that d/h varies does not yield any improvement in fuel utilization. Indeed, the systems with $d/h > 1$ (Case 2-1-05-1-05 and Case 2-1-05-15-05) show the worst fuel utilizations because the reactants are largely confined to the channel region, as discussed above. Mixing of the anode fluid and proton-conducting fluid through the small passage helps to increase fuel utilization by reducing the width of the concentration boundary layer, and ultimately minimizes the amount of unreacted fuel passing through the system. These results are consistent with the previous finding that narrowing the channel can increase the fuel utilization [6]. In addition, introducing a third stream of fluid containing electrolyte can also increase the fuel utilization up to 65% by forcing the reactants closer to their respective

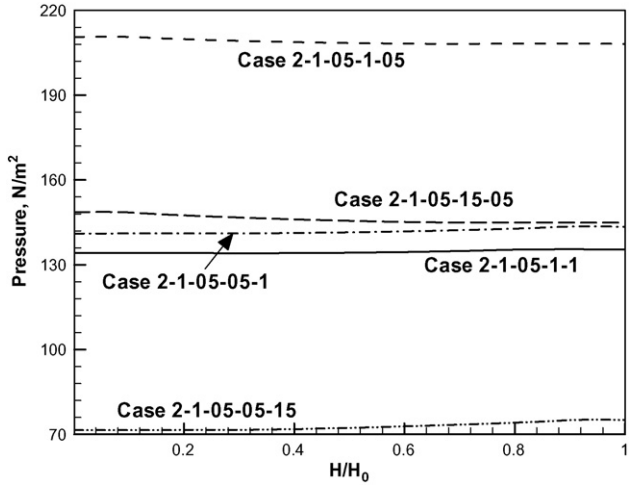

Fig. 6. Fuel pressure distribution along height through middle of anode small narrow passage at 0.1 mm downstream of first mixing point.

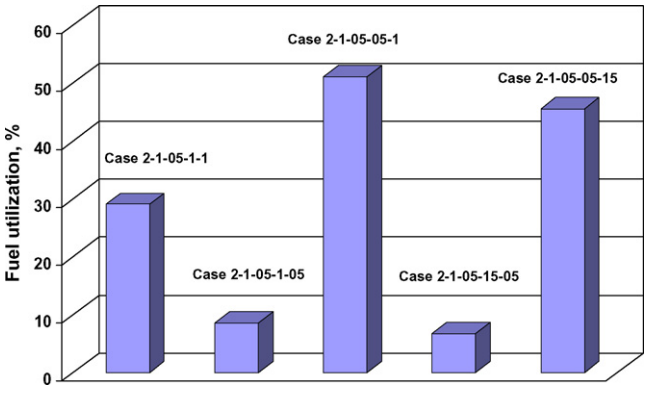

Fig. 8. Fuel utilization for different cases of Set 1.

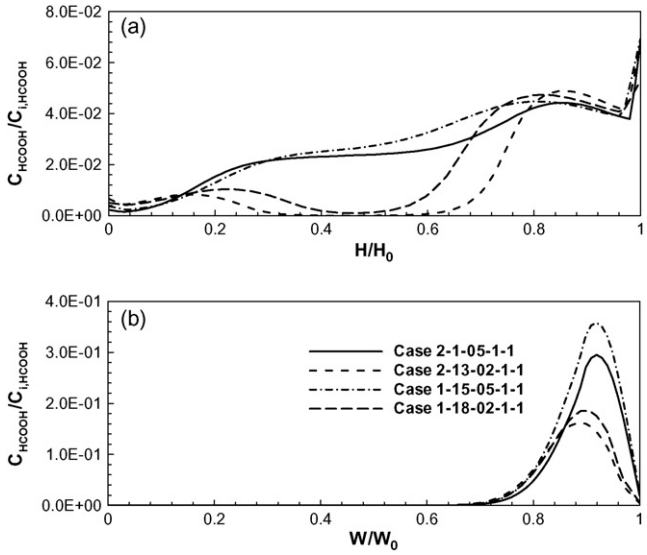

Fig. 9. Formic acid molar concentration distributions for $d/h = 1$ for different Sets: (a) parallel to the reaction surface; (b) normal to reaction surface.

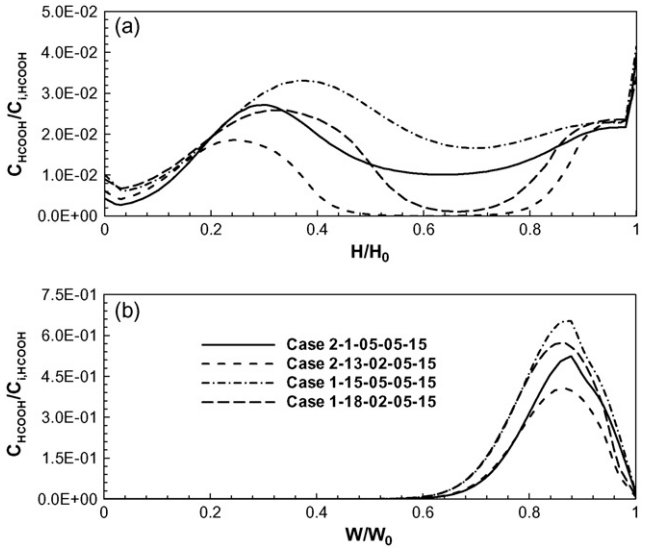

Fig. 11. Formic acid molar concentration distributions for $d/h = 1/3$ for different Sets: (a) parallel to reaction surface; (b) normal to reaction surface.

electrode boundary layers [6]. The present geometrical design with a small narrow passage and a third channel for the proton-conducting fluid generates a better distribution of reactants over the reaction surfaces.

Given that the fuel utilization is much less for systems with $d/h > 1$, only systems with $d/h \leq 1$ are now considered. Figs. 9–11 show the distribution of formic acid molar concentration both parallel to the reaction surface and normal to the reaction surface through the line y–y for $d/h = 1$, $d/h = 0.5$ and $d/h = 0.33$ across Set 1 to Set 4. In each Figure, d/h remains constant (the height of the reacting fluid channel (anode and cathode) and proton-conducting fluid channel are the same for all cases), whereas the solid slab dimensions ('*a*' and '*b*') vary according to the 4 Sets, as listed in Table 1. Comparison of the data reveals that among the two different widths of small passages, the system with a wider small passage ('*c*') show a more uniform distribution of formic acid molar concentration (see Figs. 9(a), 10(a) and 11(a)) over the reaction surfaces. This may be because in systems with a narrower small passage ('*c*'), the byproduct of the reaction hinders the passage of formic acid diffusing towards the proton-conducting fluid channel. For formic acid distribution normal to the reaction surface, however, decreasing d/h causes the reactants to keep away from the respective reaction surfaces, see Figs. 9(b), 10(b) and 11(b). The fuel utilization data for the cases with $d/h \leq 1$ of all Sets are given in Fig. 12. The fuel utilization varies significantly depending on the geometrical dimensions, in particular with the width of the small passage ('*c*') and d/h. Among the systems, the maximum fuel utilization is around 51%. It should be noted that this value is achieved using a system with a reaction area of each electrode of 0.35×10 ($L = 10$ mm) for $d/h = 0.5$, which is much smaller than those of previously reported membraneless micro fuel cells [10].

The performance of a membraneless micro fuel cell is significantly influenced by the fluid velocity in the channel as well as the reaction area. Here, only Case 2-1-05-05-1 ($d/h = 0.5$) is considered, i.e., the system that gives maximum fuel utilization (51%). To evaluate the effect of fluid velocity on the present geometrical design, Case 2-1-05-05-1 of Set 1 is modelled using different inlet velocities for all three inlets (anode, cathode and proton-conducting fluid). The influence of velocity on the reactant (formic acid) distributions parallel and normal to the reaction surface at 2 mm upstream of the outlet is presented in Fig. 13. The data show that as the velocity

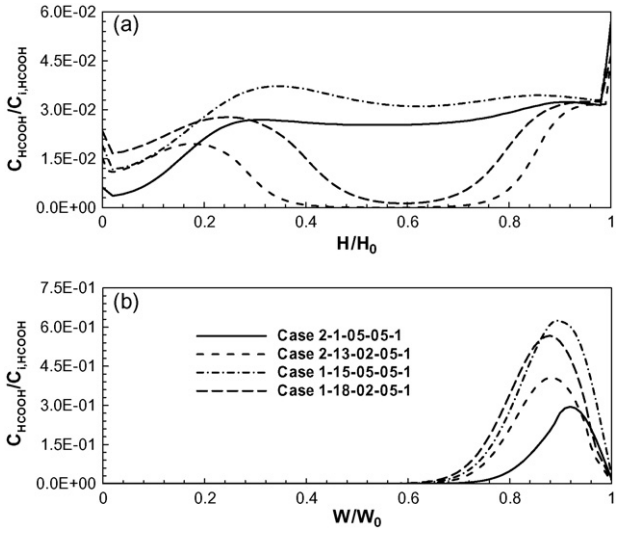

Fig. 10. Formic acid molar concentration distributions for $d/h = 1/2$ for different Sets: (a) parallel to reaction surface; (b) normal to reaction surface.

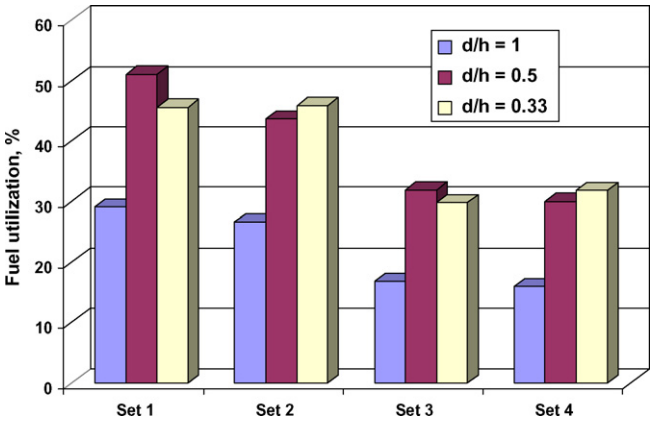

Fig. 12. Fuel utilization of different cases from all Sets.

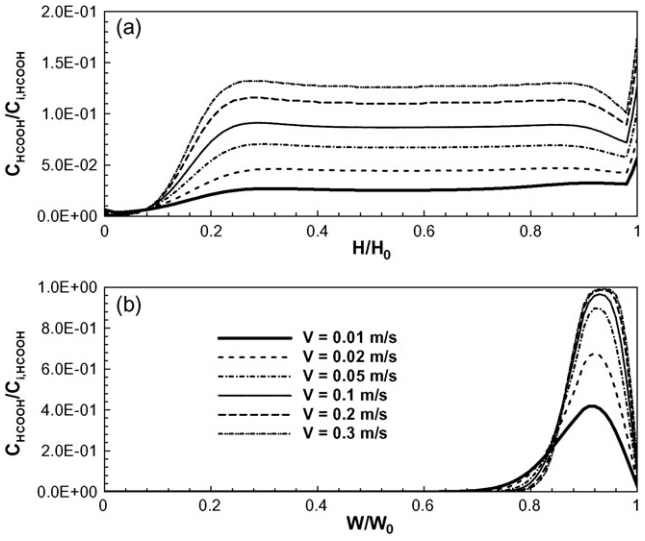

Fig. 13. Formic acid molar concentration distributions for Case 1-15-05-05-1 of Set 1 for different inlet velocities: (a) parallel to reaction surface; (b) normal to reaction surface.

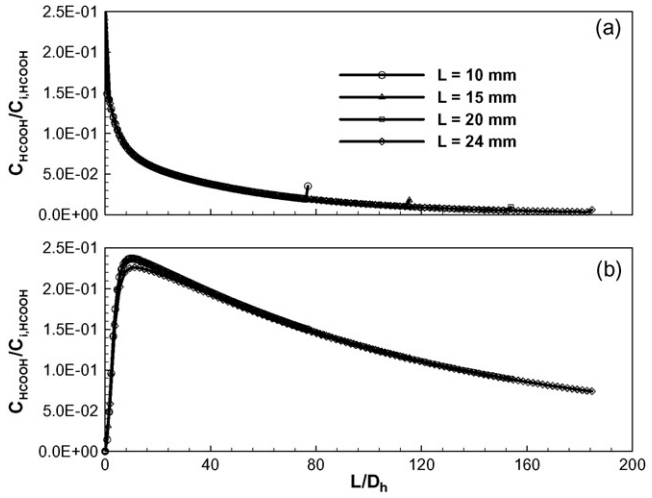

Fig. 15. Formic acid molar concentration distributions along length for Case 2-1-05-05-1: (a) $z=(h+a/2)$, $y=W$; (b) $z=h/2$, $y=c+a+2b+c/2$.

increases, less formic acid takes part in the chemical reaction and the concentration of formic acid at the reaction surface increases (parallel to the reaction surface). On the other hand, the results in Fig. 13(b) demonstrate that the concentration of formic acid is much higher in the small passage zone and the formic acid is less diffusive with the proton-conducting fluid in systems with higher inlet velocities. Fig. 14 shows the fuel utilization for Case 2-1-05-05-1 at various inlet velocities. At lower velocity, the reactants diffuse larger distances in the channel and are better distributed over the reaction surface, and have sufficient time for the chemical reaction. At higher inlet velocities, on the other hand, fewer reactant molecules impinge upon the reaction surface and hence the fuel utilization decreases significantly. A similar trend in fuel utilization as a function of inlet velocity was observed by Bazylak et al. [10]. Nevertheless, the present geometrical design gives much higher fuel utilization than can be achieved using the conventional rectangular channel cross-section, especially at low inlet velocities.

Reaction surface area is another key determinant of cell performance. To test the effect of this parameter, a comparison was made of the results of numerical simulations of systems with channel lengths of 10, 15, 20 and 24 mm. The concentration of formic acid decreases monotonically with moving downstream along its reaction surface, see Fig. 15(a), but increases sharply at the initial region of the channel at the proton-conducting fluid channel and then gradually decreases along the channel length (see Fig. 15(b)). This initial rapid increase in formic acid concentration can be attributed to the pressure gradient that develops in the initial region for $d/h<1$, as explained above. The fuel utilization data for the various channel lengths are presented in Fig. 16. The fuel utilization increases with the channel length, with a maximum value of around 70% for the channel of length 24 mm. This utilization is considerably higher than that of 52% previously achieved using a conventional rectangular channel length of 24 mm [10]. In addition, the present geometrical design has better capacity to increase the reaction surface area rather than the aspect ratio (width to height) for membraneless micro fuel cell applications. For example, it is possible to use the top surfaces of the anode and cathode channels (AE and CF in Fig. 1(b) as reaction surfaces. Moreover, a portion of the bottom surfaces of the proton-conducting fluid channel (BK and DN in Fig. 1(b)) could potentially be used as reaction surfaces (as the reactants hardly move to the opposite reaction surfaces). To test the improvements in fuel utilization that could be achieved by expanding the reaction surfaces in this way, further

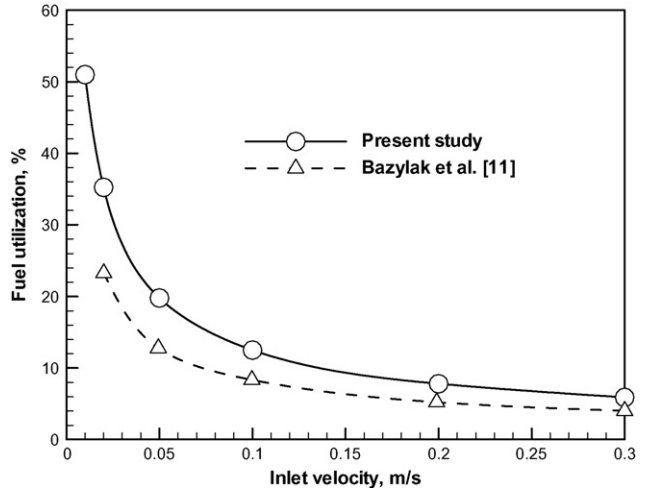

Fig. 14. Fuel utilization for Case 2-1-05-05-1 of Set 1.

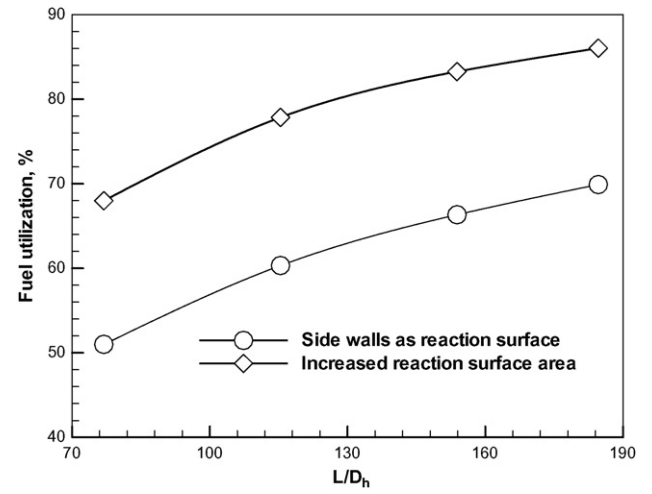

Fig. 16. Fuel utilization for Case 2-1-05-05-1 of Set 1 for different channel lengths.

computational analyses were performed with increased reaction surface areas. Specifically, the top surfaces AE and CF ($b+c$) of both the anode and the cathode channels were used as the reaction surfaces for the respective electrochemical reactions (see Table 1 and Fig. 1), respectively. In the same way, the bottom surfaces BK and DN ($b+c$) of the proton-conducting fluid channel from the respective side walls were employed as reaction surfaces. Using these expanded reaction surface areas, a fuel utilization of around 86% is achieved, as demonstrated in Fig. 16. These findings indicate that the present geometrical design can be very useful for optimizing the reactions in membraneless micro fuel cells.

Electric current, which is produced in the cell, depends on many parameters including the concentration gradients of reactants over the electrode surfaces and the effective electrochemical reaction. The present geometrical design offers better distribution of the reactants over the electrodes. The streamline for the electric field in the middle of the main channel is shown in Fig. 17(a) for Case 2-1-05-05-1 at an operating cell potential 0.4 V. Fig. 17(b) and (c) shows the electric field distributions along the two lines a–a and b–b, respectively, as pointed in Fig. 17(a). The electric fields are much higher in the proton-conducting fluid channel. Fig. 18 gives the local current density distribution along the length of the cell on the anode electrode surface at $H = 0.1$ mm, which is the top of the proton-conducting fluid channel. As the formic acid and oxygen are much less at the interface of the proton-conducting fluid channel and the small passage, especially at the inlet region, the formic acid and oxygen gradually increase along the length due to mixing. The local current density displays a similar trend as it increases along the length and then decreases as depletion occurs for formic acid and oxygen along the channel length. Note that the parameters for the electrochemical kinetics chosen from the model

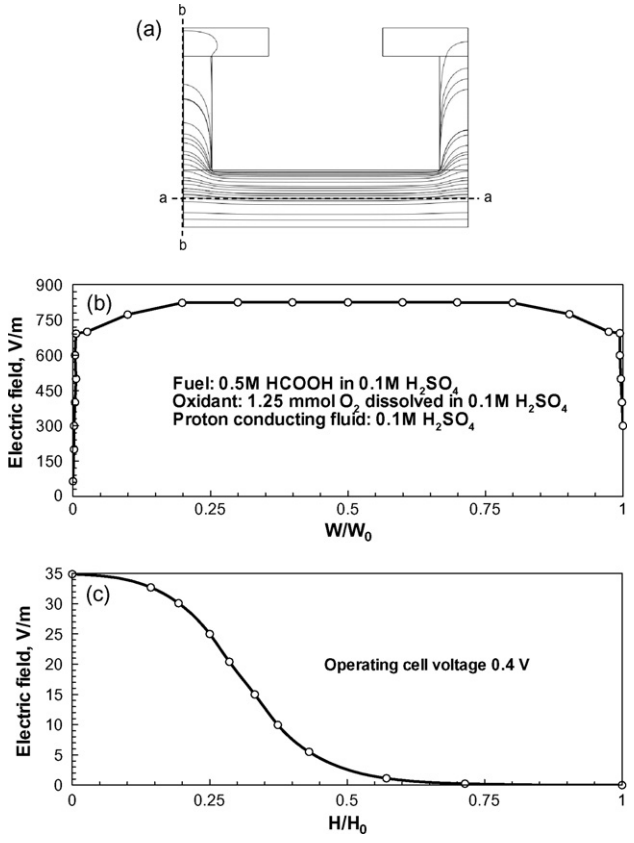

Fig. 17. (a) Streamline of electric field for Case 2-1-05-05-1 of Set 1; (b) electric field profile along line a–a; (c) electric field profile along b–b.

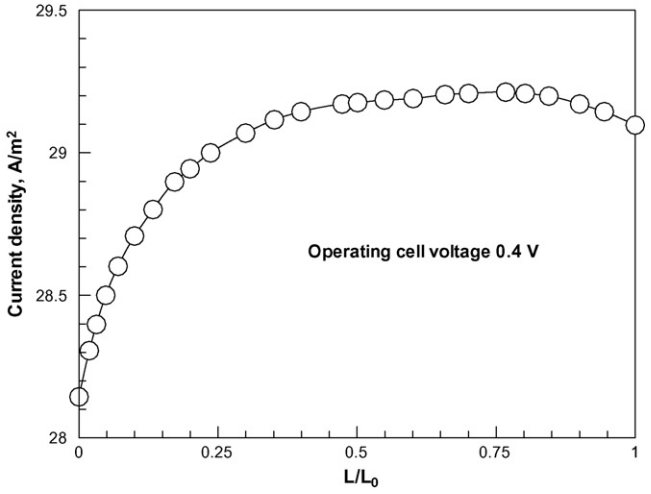

Fig. 18. Local current density distribution along length on anode electrode surface for Case 2-1-05-05-1 of Set 1.

may vary widely and the cell performance can be changed as most of the parameters exert an influence on each other.

Membraneless micro fuel cells are mainly attracting attention as alternative power sources for portable devices such as cell phones (mobile phones), cameras, and so on. Many such appliances, however, undergo continual random motions, which could stimulate mixing of the reactants in the cell. It is thought that the present geometrical design helps to minimize such mixing because the anode and cathode fluids are trapped in their respective channels to a much greater degree than is the case in conventional rectangular channels. In addition, although the gravitational effect is not considered in the present study, it is likely that gravitational forces will stimulate less movement of liquids within the cell to the incorrect sides in this geometrical design.

5. Conclusions

In the present study, a three-channel geometrical configuration is proposed for a membraneless micro fuel cell, where the three channels carry the anode, cathode and proton-conducting fluids. In this design, the anode and cathode fluids are connected by the proton-conductive fluid channel. In addition, the anode fluid and proton-conducting fluid channel are connected by a small passage and, in the same way, the cathode fluid and proton-conducting fluid channel are connected by a small passage. The major aim of the proposed geometrical design is to keep the reactants away from the opposite reaction surfaces and to increase fuel utilization in the cell. Simulation results showed that the reactants are much confined to regions near their reaction surfaces and also around the small passage zone. By the time the reactants reach the downstream region of the channel, they have diffused a distance corresponding to around 40% of the width of the proton-conducting fluid channel from their respective reaction surfaces. In addition, systems with a higher height of the proton-conducting fluid channel compared with that of the anode or the cathode fluid channel exhibit higher fluid utilization. With inlet velocities set at 0.01 m s^{-1}, it is possible to achieve 51% fuel utilization using the present geometrical design.

The numerical study has been extended to include different fluid velocities and channel lengths. Results indicate that the fuel utilization gradually decreases with increasing inlet velocities and gradually increases with increasing channel length. For a channel length of 24 mm, a maximum fuel utilization of around 70% is obtained, which is much higher than values achieved in past

studies of membraneless micro fuel cells. Moreover, the present geometrical design has a greater capacity to increase the area of the reaction surfaces on both the anode and cathode sides. Increasing the reaction surfaces by including other surfaces in addition to the side walls, the maximum fuel utilization can be increased to around 86% for a channel of length 24 mm. In addition, a higher current density can be obtained from the present design compared with the conventional geometrical design. The present geometrical configuration is a superior design for membraneless micro fuel cells, because these devices are intended for use in portable electrical appliances that undergo random motions. Further studies of the proposed system, including the electric potential equation, are necessary to characterize more precisely the performance of the proposed design.

Acknowledgements

This work was supported by the Korea Research Foundation and was partially funded by Brain Korea 21.

References

[1] R.S. Jayashree, L. Gancs, E.R. Choban, A. Primak, D. Natarajan, L.J. Markoski, P.J.A. Kenis, J. Am. Chem. Soc. 127 (2005) 16758–16759.
[2] D.H. Ahmed, H.J. Sung, J. Power Sources 162 (2006) 327–339.
[3] D.H. Ahmed, H.J. Sung, Int. J. Heat Mass Transfer (2007).
[4] H. Tsuchiya, O. Kobayashi, Int. J. Hydrogen Energy 29 (2004) 985–990.
[5] J.L. Cohen, D.J. Volpe, D.A. Westly, A. Pechenik, H.D. Abruna, Langmuir 21 (2005) 3544–3550.
[6] E.R. Choban, L.J. Markoski, A. Wieckowski, P.J.A. Kenis, J. Power Sources 128 (2004) 54–60.
[7] R. Ferrigno, A.D. Stroock, T.D. Clark, M. Mayer, G.M. Whitesides, J. Am. Chem. Soc. 124 (2002) 12930–12931.
[8] F. Chen, M.H. Chang, C.W. Hsu, Electrochim. Acta 52 (2007) 7270–7277.
[9] J.L. Cohen, D.A. Westly, A. Pechenik, H.D. Abruna, J. Power Sources 139 (2005) 96–105.
[10] A. Bazylak, D. Sinton, N. Djilali, J. Power Sources 143 (2005) 57–66.
[11] M.H. Chang, F. Chen, N.S. Fang, J. Power Sources 159 (2006) 810–816.
[12] T.J. Kemp, W.A. Waters, Proc. R. Soc. Lond., Ser. A, Math. Phys. Sci. 274 (1359) (1963) 480–499.
[13] J. Jiang, A. Kucernak, J. Electroanal. Chem. 520 (2002) 64–70.
[14] A.V. Tripkovic, K.Dj. Popovic, J.D. Lovic, N.M. Markovic, V. Radmilovic, Mater. Sci. Forum 494 (2005) 223–228.
[15] L.B. Younis, J. Energy Institute 79 (4) (2006) 222–227.
[16] A.B. Anderson, J. Roques, S. Mukejee, V.S. Murthi, N.M. Markovic, V. Stamenkovic, J. Phys. Chem. B 109 (2005) 1198–1203.
[17] W.E. Mustain, K. Kepler, J. Prakash, Electrochim. Acta 52 (2007) 2102–2108.
[18] F. Chen, M.H. Chang, M.K. Lin, Electrochim. Acta 52 (2007) 2506–2514.
[19] G.E. Walrafen, W.–H. Yang, Y.C. Chu, M.S. Hokmabadi, J. Solution Chem. 29 (10) (2000) 905–936.